Ultrathin MoS₂ Nanosheets for Electrocatalytic N₂-To-NH₃ Fixation Under Ambient Conditions

Yanmei Liao, Weijun Ye, Yinghong Zhu[*], *Lianbang Wang*[*]

College of chemical Engineering, Zhejiang University of Technology, Hangzhou, 310023 Zhejiang China
[*]E-mail: yhzhuchem@zjut.edu.cn, wanglb99@zjut.edu.cn

Electrochemical N_2 reduction reaction (NRR) provides a quite potential method for ammonia (NH_3) synthesis under ambient conditions, while it requires efficient and durable catalysts. In this communication, we report an ultrathin nanosheets MoS_2 that acts as electrocatalyst for NRR, which assumed excellent selectivity. In 0.1 M Na_2SO_4 with N_2-saturation under ambient conditions, this electrocatalyst at -0.6 V vs. reversible hydrogen electrode (RHE) exhibited a large NH_3 yield of 41.66 $\mu g\ h^{-1}\ mg^{-1}_{cat.}$ and a Faradaic efficiency (FE) of 1.10%. Furthermore, the electrochemical stability is also exhibiting excellent.

1. INTRODUCTION

NH_3 is not only an important chemical in the production of fibres, resins, fertilizers and explosives [1-6], but it also a conveniently hydrogen carrier with high-energy density and zero CO_2 emission. Even though N_2 is the most abundant gas on the earth, but it is extremely hard to convert into NH_3, due to the difficulty to cleave inertness of the N≡N triple bond [7-9]. In industrially, NH_3 is synthesized by the conventional Haber-Bosch process at harsh reaction conditions. This synthesis method consumes considerable energy sources, causing huge CO_2 emissions. Therefore, it is high urgency to develop sustainable and economical routes for synthesis of NH_3 under room conditions.

Recently, NRR produced NH_3 has aroused abundant research interest [10-34]. Noble metals including Au [22], Pd [23], Pt [24] and Ru [25] present favourable catalytic performance for the electrocatalytic NRR. However, such metals are rare and the price is high. In nature, Mo is known as the active centre in nitrogenases and has a very low potential determining step (PDS) value through the enzymatic pathway [35], which is proved to be the most successful element for homogeneous N_2

functionalization reactions. Thus, to design and synthesize the molecular complexes for N_2 reduction have considerable to pay much attentions. Yang et al.[13] reported the use of Mo nanofilm as an catalyst for NRR with the NH_3 yield of 1.89 μg h^{-1} cm^{-2}. Recently, molybdenum disulphide (MoS_2) has been also as active for NRR, due to possessing is a layered graphene-like structure, low-cost, relatively non-toxic and good stability of liquid medium. MoS_2 is firstly reported being used as electrocatalyst of NRR under room temperature and atmospheric pressure, and the NH_3 yield of 8.08×10^{-11} mol s^{-1} cm^{-1} [12]. Furthermore, defect-rich MoS_2 nanoflowers and MoS_2 nanosheet–reduced graphene oxide hybrids (MoS_2-rGO) were reported for NRR, with the NH_3 yield of 29.28 μg h^{-1} mg^{-1}cat. and 24.82 μg h^{-1} mg^{-1}cat., respectively [15,31]. Nonetheless, the hydrogen evolution reaction (HER) is known as the major side reaction of the NRR, will reduce the activity and FE of the NRR.

In this communication, an ultrathin nanosheet of MoS_2 was synthesized by sol–Gel-like method and used as the electrocatalyst for NRR at ambient conditions, in N_2-saturation of 0.1 M Na_2SO_4 solution present excellent activity.

2. EXPERIMENTAL

2.1. Materials

Anhydrous ethanol was purchased from Aladdin Ltd. (Shanghai, China). Sulfuric acid (H_2SO_4), sodium hydroxide (NaOH), sodium sulfate (Na_2SO_4), ammonium molybdate ((NH_4)$_6$Mo$_7$O$_{24}$·4H$_2$O), urea (CH_4N_2O), thiourea (CH_4N_2S), hydrogen peroxide (H_2O_2), hydrazine hydrate (N_2H_4·H$_2$O), ammonium chloride (NH_4Cl), sodium citrate dehydrate ($C_6H_5Na_3O_7$·2H$_2$O), sodium nitroferricyanide dihydrate ($C_5FeN_6Na_2O$·2H$_2$O), dimethylaminobenzaldehyde ($C_9H_{11}NO$), Nafion (5wt.%) and sodium hypochlorite solution (NaClO) were purchased from Sigma-Aldrich Chemical Reagent Co. Ltd. All reagents were analytical grades, and without further purification. The type of carbon cloth (CC) in test is Shanghai Hesen Electric Co. Ltd (HCP030N). The Ar/N_2 gas purify is 99.999%). The water was purified by a Millipore system.

2.2. Synthesis of MoS$_2$ nanosheets

The nanosheet of MoS_2 was synthesized by similarly Sol-Gel method. As a typical synthesis, 0.46 g of ammonium molybdate, 0.5 g of thiourea, 5 g of urea, 25 mL of deionized water and 75 mL of anhydrous ethanol were added into 150 mL beaker, respectively. After stirring for about 30 min, a transparent solution was obtained, the solution was heated to 75 ℃ until the solution remaining after about 5 mL, then it was dried in an oven at 100 ℃ for overnight until get dry precipitation product. Finally, the dried precipitate was calcined in Ar with the heating rate 5 ℃ min^{-1} at 350 ℃ for 4 h and then heat up to 650 ℃ for 10 h to get the nanosheet MoS_2.

2.3. Preparation of catalyst electrodes

MoS_2 deposited on carbon cloth (CC) electrode as the working electrode (MoS_2/CC MoS_2 loading: 0.1 mg cm^{-2}). Typically, 10 mg of catalyst were dispersed in 950 µL solution containing ethanol and H_2O (volume ration :1/1), then added 50 µL of Nafion solution (5 wt.%) into the mix suspension for sonicated 1 h to form a homogeneous solution. And then, 10 µL of homogeneous solution was immediately droped onto the carbon cloth electrode with area of 1×1 cm^2 and dried under ambient condition. The MoS_2/CC electrode was prepared well.

2.4 Characterization

The phase purity of the as-synthesized samples was analyzed by X-ray diffraction (XRD) patterns with a RIGAKU Ultimate IV diffractometer using Cu Kα radiation with 60 kV and 60 mA. Transmission electron microscopy (TEM) was obtained by using JEM-2010Ex (Japan) at an accelerating voltage of 200 kV.

2.5 Electrochemical Measurements

NRR experiments were measured under ambient condition by a two-compartment cells, and the cathode and anode cells were separated through Nafion 211 membrane. The Nafion membrane was firstly boiling in deionized water for 1 h to protonation and then treating in H_2O_2 (5%) aqueous solution for another 1 h at 80 ℃, respectively. Following, the membrane was treated in 0.5 M H_2SO_4, for 3 h at 80 ℃ and finally in water for 6 h before NRR tests. The electrochemical experiments were performed with an electrochemical workstation (CHI 660D). The three-electrode configuration including prepared electrode as working electrode, 2×2 cm^2 Pt foil as counter electrode and Ag/AgCl electrode (saturated KCl solution) as reference electrode, respectively. The potentials electrode in this work were converted to RHE scale, calibration by the following equation: E (vs. RHE) =E (vs. Ag/AgCl) + 0.059×pH+0.197 V, and the current desity was normalized to the geometric surface area. The chronoamperometry tests were conducted for electrochemical NRR.

2.6 Calculation of ECSA

The electrochemically active surface area (ECSA) was determined by double layer capacitance method. CV measurement was conducted at -0.6V~-0.8 V vs. Ag/AgCl with various scan rates of 20, 40, 60, 80, 100 mV s^{-1}. By plotting the (j_a -j_c)/2 at -0.70 V vs. Ag/AgCl against the scan rate, the slope value was calculated to be the double layer capacitance (C_{dl}).

2.7 Determination of NH$_3$

The concentration of ammonia was estimated by ultraviolet-visible (UV-vis) spectrophotometry using the indophenol blue method. In a typical run, 0.5 mL of solution containing NaOH (0.32 M) and

sodium salicylate (0.4 M), 50 μL of solution containing NaClO (0.05 M) and NaOH (0.75 M), and 50 μL of $C_5FeN_6Na_2O$ (1wt.%) added into 4 mL of the electrolyte, and was mixed homogeneous avoid light for 1 h. The UV-vis absorption spectrum was recorded on a UV1004M009 spectrophotometer. The absorbance was determined at $\lambda=680\sim$ nm. The concentration-absorbance curves were calibrated using standard ammonia chloride solution with NH_4^+ concentrations of 0.00, 0.05, 0.10, 0.15, 0.20, 0.25 and 0.30 μg ml^{-1} in 0.1 M Na_2SO_4. The fitting curve (y=0.722x+0.0108, R^2=0.997) showed good linear relation of absorbance value with NH_3 concentration by three times independent calibrations. The NH_3 yield was calculated using the following equation:

$$C_{NH3}=(V\times[NH_3])/(m_{cat}\times t)$$

Where C_{NH3} (μg mL^{-1}) is the mass produced NH_3 concentration, V (mL) is the volume of the Na_2SO_4 electrolyte, t (h) is the reduction reaction time and m (mg) is the loading mass of catalysts.

2.8 Determination of N_2H_4

The method of Watt and Chrisp was measured to detected N_2H_4. The color reagent was prepared by mixing 300 mL of ethanol (300 mL), concentrated HCl (30 mL) and *p*-(dimethylamino)benzaldehyde (5.99g). The absorbance of the resulting solution was measured at $\lambda= 456\sim$ nm, and the yield of N_2H_4 were calculated from the standard curve using the 5 mL of the electrolyte and 5 mL of color reagent were mixed for 20 min. The $N_2H_4 \cdot H_2O$ solution were as a standard for absolute calibration of this method, and the fitting curve showed a good linear relation of absorbance with the N_2H_4 concentration (y=0.561x+0.0320, R^2=0.999) by three times' independent calibrations.

2.9 Faradaic efficiency

The FE of the NRR is defined as the amount of electric charge used for synthesizing NH_3 divided by the total charge passed through the electrodes during electrolysis. Assuming three electrons are needed to produce one NH_3 molecule, the faradaic efficiency can be calculated as follows:

$$FE=(3F\times V\times[NH_3])/(Q\times17)$$

Where F (96485 C mol^{-1}) is the Faraday constant, NH_3 (mol) is the number of moles of produced NH_3 and Q (C) is the total electric charge during the whole NRR process.

3. RESULTS AND DISCUSSION

3.1. Characterization of MoS_2 nanosheets

The X-ray diffraction (XRD) pattern of MoS_2 sample was showed in Fig.1a. The peaks at 13.78º, 33.44º, 39.65º and 58.55º are assigned to (002), (100)+(101), (103), and (110) of MoS_2, respectively (JCPDS No.73-1508).
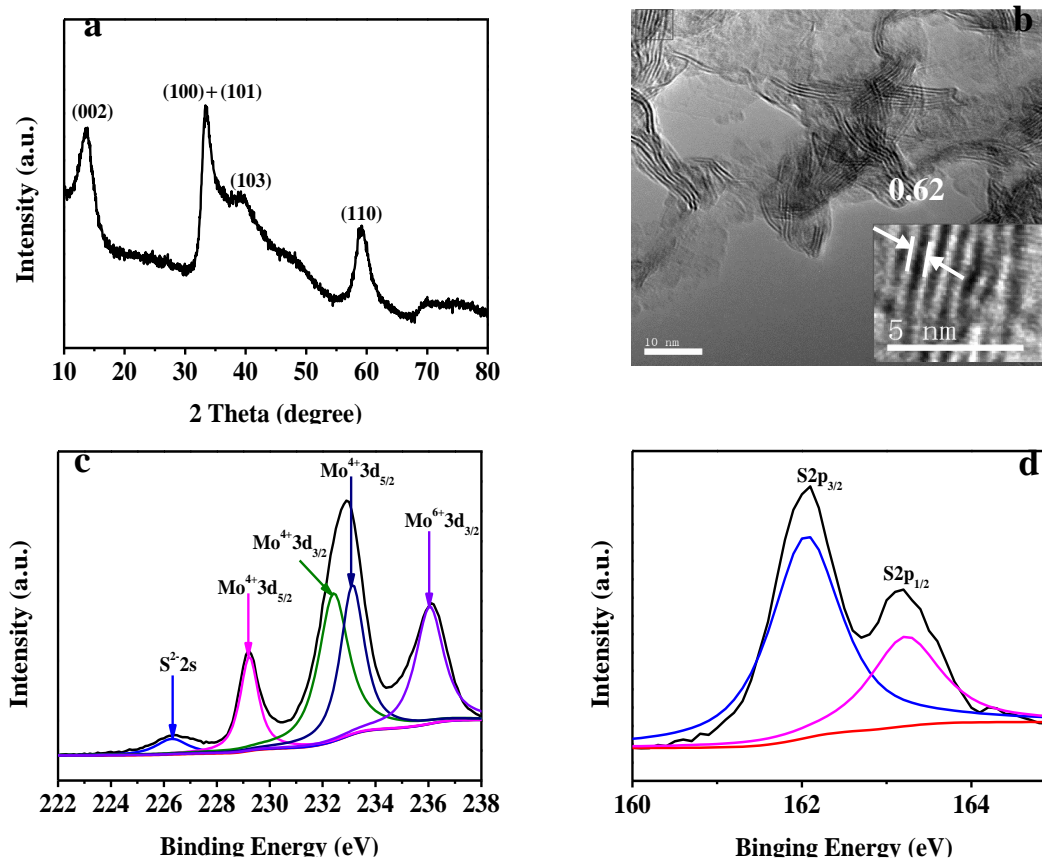
Figure 1. (a) The XRD pattern of MoS_2 sample. (b) The TEM image of MoS_2 and XPS spectra of MoS_2 sample in the Mo 3d (c) and S 2p (d) regions.

Fig.1b presents the transmission electron microscopy (TEM) image, which exhibits a lamellar morphology consisting of 3-6 layers S-Mo-S and the lattice spacing of 0.62 nm corresponding to (002) plane. The X-ray photoelectron spectroscopy (XPS) spectra of Mo 3d and S 2p regions was displayed in Fig. 1c and 1d. The binding energies (BEs) at 228.7, 231.8, 232.8 and 235.7 eV are assigned to Mo^{4+} and Mo^{6+}. The binding energy at 225.9 eV is confirmed to the presence of sulphur in the MoS_2 structure [36]. The BEs at 162.3 and 163.5 eV are assigned to S $2p_{3/2}$ and $2p_{1/2}$, respectively, consistent with the S^{2-}.

### 3.2. Electrochemical Performance

The NRR electrochemical performance were carried out using a typical three-electrode system, the produced NH_3 and the possible by-product N_2H_4 were determined by spectrophotometry with an indophenol blue method [37], dimethylaminobenzaldehyde [38], respectively. The corresponding calibration curves of NH_3 and N_2H_4 were showed in Fig.2.
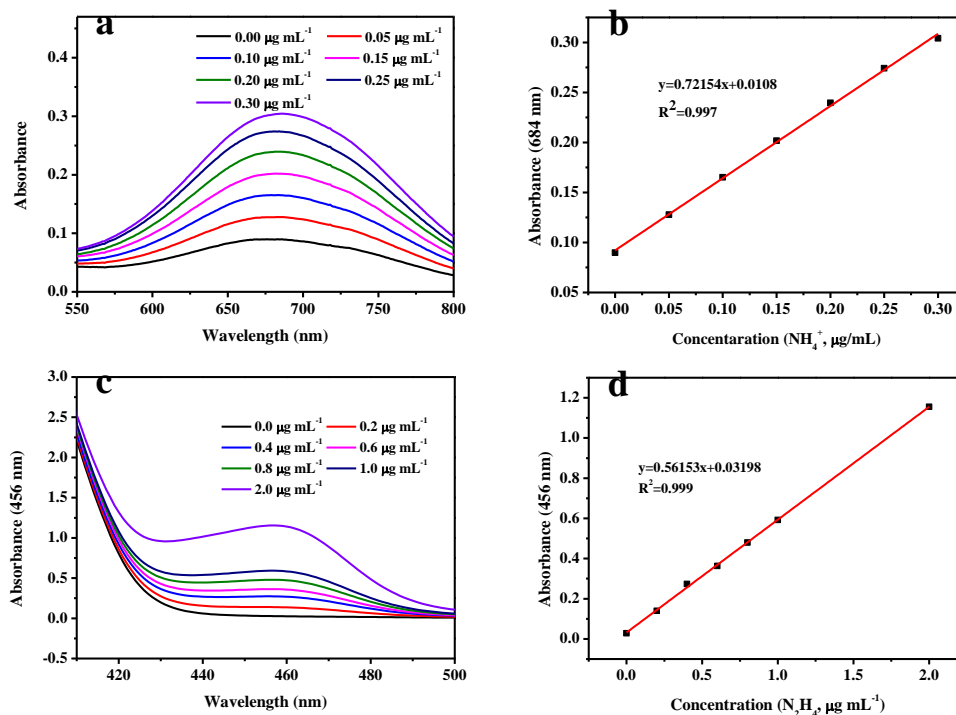
Figure 2 (a) The UV-Vis absorption spectra of indophenol assays with NH_4^+ ions after incubated for 1 h at room temperature. (b) Calibration curve used for estimation of NH_4^+ ion concentration. (c) The UV-Vis absorption spectra of different N_2H_4 concentrations after incubation for 20 min at room temperature. (d) Calibration curve used for calculation of N_2H_4 concentrations.

Fig. 3a exhibits the linear sweep voltammetry (LSV) curves under N_2- and Ar-saturated 0.1 M Na_2SO_4 solutions. It is obviously seen that MoS_2/CC attains higher current density in N_2-saturated solution, indicating that MoS_2/CC has catalytic activity for the NRR. Fig. 3b shows the UV-Vis spectra after electrolysis 2h, demonstrating the NRR can be occurred from -0.3 to -0.7 Von MoS_2/CC electrode. Remarkably, the maximum absorbance at -0.6 V, suggesting that the MoS_2/CC can achieve the highest NH_3 yield at this potential. Fig. 3c presents the current density curves at various potentials, and the current density almost remains constant, indicating their excellent stability under 2 h electrolysis in N_2-saturated electrolytes. Fig. 3d illustrates the average NH_3 yields and FEs. It is clearly seen that the parameters increase from -0.3 until -0.60 V, where the maximum NH_3 yield and FEs were achieved, 41.66 μg h^{-1} mg$^{-1}_{cat.}$ and 1.10%, respectively. Fortunately, the NH_3 yield is higher than most reported electrocatalysts, including MoS_2/CC (8.08×10^{-11} mol s^{-1} cm^{-1}) [12], Mo nanofilm (1.89 μg h^{-1} cm^{-2}) [13], Pd/C (4.5 μg h^{-1} mg$^{-1}_{cat.}$) [23], and MoS_2-rGO (24.82 μg h^{-1} mg$^{-1}_{cat.}$) [31]. The more detailed comparisons are displayed in Table 1. To understand the origin of the enhanced NRR activity, surface areas were measured for the samples using electro-chemical double-layer capacitance [39], as shown in Fig. 4. The electrochemically active surface area (EASC) is calculated to1.7 mF cm^{-2}, which was higher than MoS_2-rGO (0.065 mF cm^{-2}) [31]. The NH_3 yield and FE increased from -0.30 to -0.60 V, while the potential is negatively shifted over -0.60 V, the NH_3 yield and FE decreased obviously. This may be the competitive on the electrode surface of adsorption nitrogen and hydrogen [40, 41]. The NRR on MoS_2 surface may

follow the associative mechanism, and the nitrogen molecules are gradually reduced with protons and electrons [42].
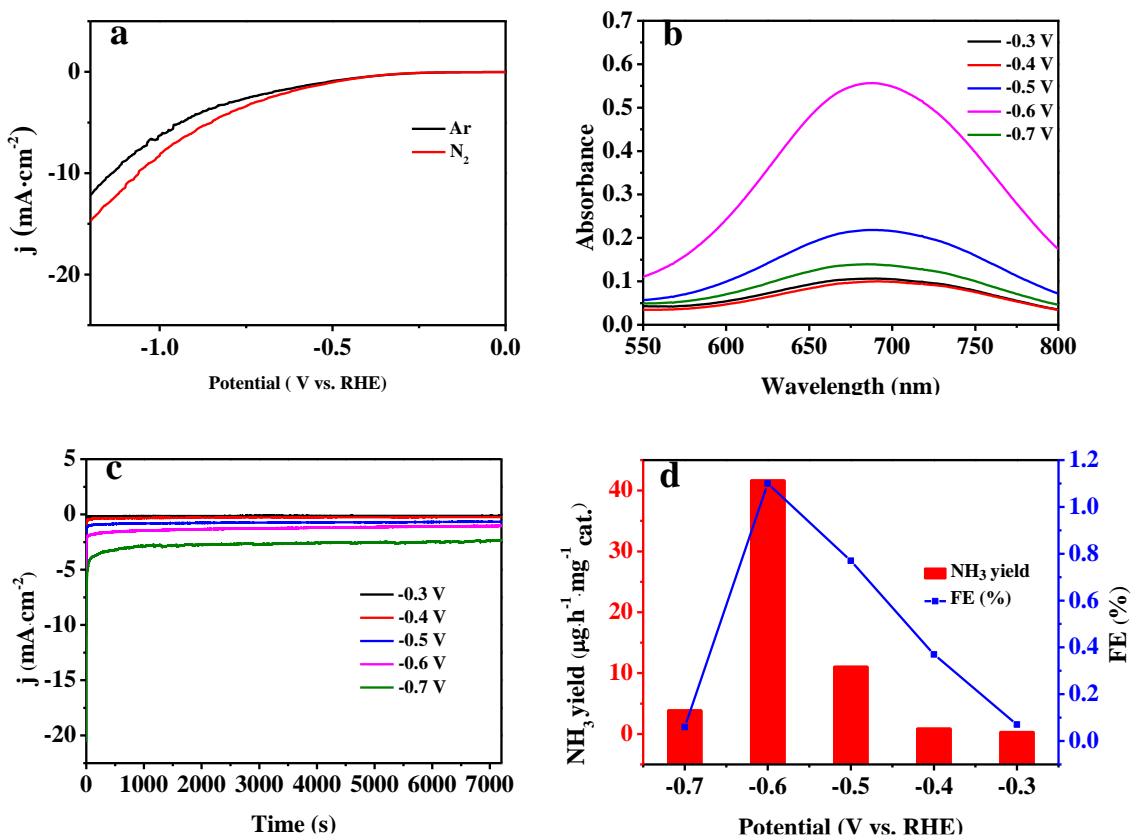
Figure 3. (a) The LSV curves in Ar- and N_2- saturated 0.1 M Na_2SO_4 at scan rate of 5 mV s^{-1} of MoS_2/CC. (b) The UV-vis absorption spectra of electrolytes after electrolysis for 2 h at series potentials. (c) The Time-dependent current density curves at various potentials in N_2-saturated 0.1 M Na_2SO_4 electrolyte of MoS_2/CC. (d) The NH_3 yields and FEs at series potentials of MoS_2/CC.
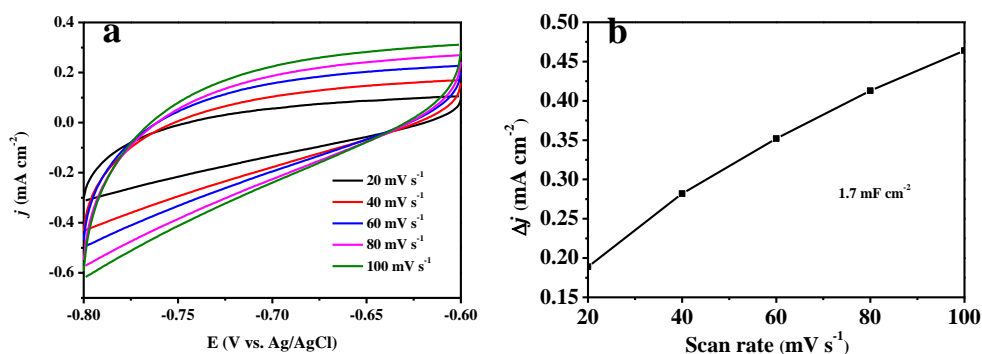

Figure 4. (a) The CVs and (b) The capacitive current densities of MoS_2/CC.

In order to verify the NH_3 was indeed produced from electrocatalytic NRR over MoS_2, we also measured the electrolysis in a N_2-saturated/Ar-saturated solution with no applied voltage.

**Table 1.** Comparison of various electrocatalyst for NRR performance to our MoS_2 at room temperature.

| Catalyst	Electrolyte	NH_3 yield	FE (%)	Ref.
MoS_2	0.1 M Na_2SO_4	41.66 µg h^{-1} mg^{-1} cat.	1.10	This work
Ag nanosheet	0.1 M HCl	4.62×10^{-11} mol s^{-1} cm^{-2}	4.80	43
Ru/C	2.0 M KOH	0.21 µg h^{-1} cm^{-2}	0.28	44
Oxygen-doped carbon nanosheet	0.1 M HCl	20.15 µg h^{-1} mg^{-1} cat.	4.97	45
MoS_2-rGO	0.1 M $LiClO_4$	24.82 µg h^{-1} mg^{-1} cat.	4.58	31
La_2TiO_7	0.1 M HCl	25.15 µg h^{-1} mg^{-1} cat.	4.55	46
$K_2Ti_4O_9$ nanobelt	0.1 M KOH	22.88 µg h^{-1} mg^{-1} cat.	8	47
Nb_2O_5	0.1 M Na_2SO_4	1.58×10^{-10} mol s^{-1} cm^{-2}	2.26	48
Au flower	0.1 M HCl	25.57 µg h^{-1} mg^{-1}cat.	6.05	49
Fe_3O_4 nanorod	0.1 M Na_2SO_4	5.6×10^{-11} mol s^{-1} cm^{-2}	2.60	50
Ag_3Cu	0.1 M Na_2SO_4	24.59 µg h^{-1} mg^{-1}cat.	13.28	51
MoS_2 Nanoflower	0.1 M Na_2SO_4	29.28 µg h^{-1} mg^{-1}cat.	8.34	15
Cr_2O_3	0.1 M HCl	28.13 µg h^{-1} mg^{-1}cat.	8.56	52
Cu-CeO_2-3.9	0.1 M Na_2SO_4	5.3×10^{-10} mol s^{-1} cm^{-2}	19.1	53
TiS_2 nanosheets	0.1 M Na_2SO_4	16.02 µg h^{-1} mg^{-1}cat.	5.5	54
Mo nanofilm	0.01 M H_2SO_4	1.89 µg h^{-1} cm^{-2}	0.72	13
MoS_2/CC	0.1 M Na_2SO_4	8.08×10^{-11} mol s^{-1} cm^{-2}	1.17	12
Pd/C	0.1 M PBS	4.5 µg h^{-1} mg^{-1}cat.	8.2	23
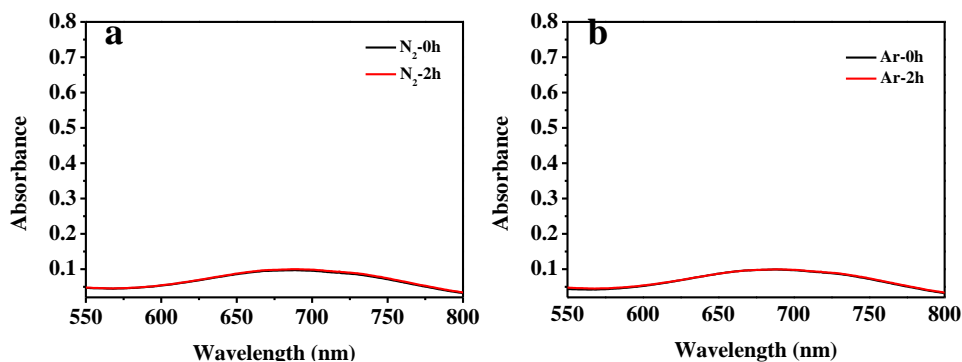
Figure 5. The UV-Vis absorption spectra of 0.1 M Na_2SO_4 electrolytes stained with indophenol indicator after continuously supplying (a) N_2 and (b) Ar with no applied voltage.

It is clear that there were almost no differences of the corresponding UV-vis spectra for both cases, between before and after electrolysis (Fig.5), suggesting there are no NH_3 generated. Furthermore, we investigated the

CC electrode for NRR at -0.60 V for 2 h electrolysis under ambient condition. The CC electrode and MoS_2/CC electrode relevant UV-vis absorption spectra are displayed in Fig. 6a. Apparently, CC has almost no electrocatalytic activity for the NRR (Fig. 6b). These results declare that the N_2 fixation process occurs with the existence of MoS_2. There were no by-product N_2H_4 is detected in final electrolytes at all potentials (Fig. 7), which implies MoS_2 has good selectivity for NRR.
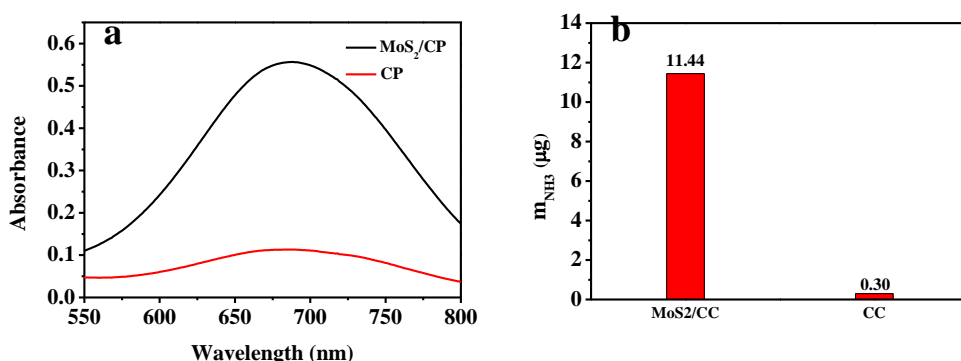
Figure 6. (a) The UV-Vis absorption spectra of electrolytes colored with indophenol indicator after electrolysis under different conditions for 2 h. (b) The amount of NH_3 produced from MoS_2/CC and bare CC after 2 h electrolysis.
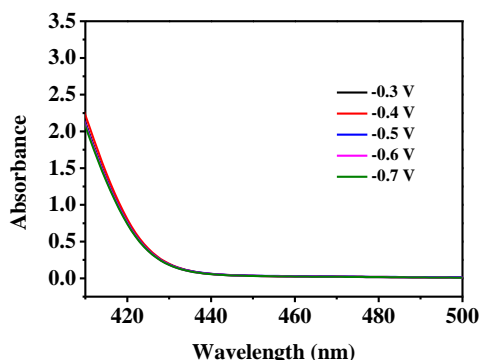
Figure 7. The UV-Vis absorption spectra of various electrolytes estimated by Watt and Chrisp method after electrolysis in N_2-saturated 0.1 M Na_2SO_4 for MoS_2/CC.
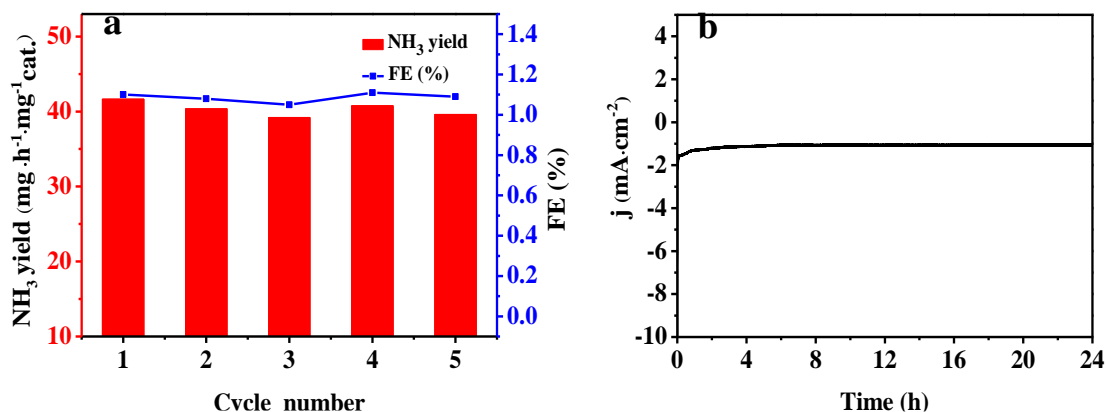
Figure 8. (a) The recycling test for MoS_2/CC at -0.60 V. (b) The MoS_2/CC of Time-dependent current density curve in N_2-saturated 0.1 M Na_2SO_4 at -0.60V for 24 h.

To evaluate the catalytic performance, durability and stability are also important factors. Fig.8a displays the recycling of NH_3 yield rates the FEs, the negligible changes during recycle tests for 5 times at -0.60 V, suggesting the MoS_2 with high activity and stability. In addition, we also tested at -0.60 V in N_2-saturated electrolyte for the long-term electrochemical stability, which reveals a stable current for the testing period of 24 h (Fig. 8b). All these results indicate that MoS_2/CC is an excellent durability and stability electrocatalyst for NRR under ambient conditions.

4. CONCLUSIONS

In conclusion, MoS_2 has been proved as a high-active, durable and with 100% selectivity electrocatalyst, for the N_2 convert to NH_3 at room temperature. The NH_3 yield is high to 41.66 μg h^{-1} mg$^{-1}_{cat.}$, and the FE is 1.10% at -0.60 V (vs. RHE) in 0.1 M Na_2SO_4. In the future, we will focus on modified MoS_2/CC electrode in order to enhance the Faradaic efficiency with excellent activity for the NRR.

References

1. R. Schlögl, *Angew. Chem., Int. Ed.*, 42 (2003) 2004.
2. V. Smil, *Nature*, 400 (1999) 415.
3. V. Rosca, M. Duca, M. T. de Groot and M. T. M. Koper, *Chem. Rev.*, 109 (2009) 2209.
4. J. N. Galloway, A. R. Townsend, J. W. Erisman, M. Bekunda, Z. Cai, J. R. Freney, L. A. Martinelli, S. P. Seitzinger and M. A. Sutton, *Science*, 320 (2008) 889.
5. X. Guo, H. Du, F. Qu and J. Li, *J. Mater. Chem. A*, 7 (2019) 3531.
6. H. Du, R.-M. Kong, X. Guo, F. Qu and J. Li, *Nanoscale*, 10 (2018) 21617.
7. V. Smil, *Sci. Am.*, 277 (1997) 76.
8. H.-P. Jia and E. A. Quadrelli, *Chem. Soc. Rev.*, 43 (2014) 547.
9. X. Zhang, R.-M. Kong, H. Du, L. Xia and F. Qu, *Chem. Commun.*, 54 (2018) 5323.
10. C. Guo, J. Ran, A. Vasileff and S.-Z. Qiao, *Energy Environ. Sci.*, 11 (2018) 45.

11. Y. Zhou, X. Yu, F. Sun and J. Zhang, *Dalton Trans.*, 49 (2020) 988.
12. L. Zhang, X. Ji, X. Ren, Y. Ma, X. Shi, Z. Tian, A. M. Asiri, L. Chen, B. Tang and X. Sun, *Adv. Mater.*, 30 (2018) 1800191.
13. D. Yang, T. Chen and Z. Wang, *J. Mater. Chem. A*, 5 (2017) 18967.
14. S.-J. Li, D. Bao, M.-M. Shi, B.-R. Wulan, J.-M. Yan and Q. Jiang, *Adv. Mater.*, 33 (2017) 1700001.
15. X. Li, T. Li, Y. Ma, Q. Wei, W. Qiu, H. Guo, X. Shi, P. Zhang, A. M. Asiri, L. Chen, B. Tang and X. Sun, *Adv. Energy Mater.*, 8 (2018) 1801357.
16. L. Zhang, X. Ji, X. Ren, Y. Luo, X. Shi, A. M. Asiri, B. Zheng and X. Sun, *ACS Sustainable Chem. Eng.*, 8 (2018) 9550.
17. X. Yu, P. Han, Z. Wei, L. Huang, Z. Gu, S. Peng, J. Ma and G. Zheng, *Joule*, 8 (2018) 1610.
18. H. Cheng, L.-X. Ding, G.-F. Chen, L. Zhang, J. Xue and H. Wang, *Adv. Mater.*, 30 (2018) 11803694.
19. Y. Liu, Y. Su, X. Quan, X. Fan, S. Chen, H. Yu, H. Zhao, Y. Zhang and J. Zhao, *ACS Catal.*, 12 (2018) 1186.
20. L. Han, X. Liu, J. Chen, R. Lin, H. Liu, F. Lü, S. Bak, Z. Liang, S. Zhao, E. Stavitski, J. Luo, R. R. Adzic and H. Xin, *Angew. Chem. Int. Ed.*, 58 (2019) 2321.
21. Z. W. Chen, X. Y. Lang and Q. Jiang, *J. Mater. Chem. A*, 6 (2018) 9623.
22. D. Bao, Q. Zhang, F.-L. Meng, H.-X. Zhong; M.-M, Shi, Y. Zhang, J.-M. Yan, Q. Jiang and X.-B. Zhang, *Adv. Mater.*, 3 (2017) 1604799.
23. J. Wang, L. Yu, L. Hu, G. Chen, H. Xin and X. Feng, *Nat. Commun.*, 1 (2018) 1795.
24. Y. Yao, S. Zhu, H. Wang, H. Li and M. Shao, *J. Am. Chem. Soc.*, 140 (2018) 1496.
25. D. Wang, L. M. Azofra, M. Harb, L. Cavallo, X. Zhang, B. H. R. Suryanto and D. R. Macfarlane, *ChemSusChem*, 11 (2018) 3416.
26. S. Wang, W. Wei, X. Lv, B. Huang and Y. Ding, *J. Mater. Chem. A*, 8 (2020) 1378.
27. M.-M. Shi, D. Bao, B.-R. Wulan, Y.-H. Li, Y.-F. Zhang, J.-M. Yan and Q. Jiang, *Adv. Mater.*, 29 (2017) 1606550.
28. J. Wang, S. Wang and J. Li, *Dalton Trans.*, 49 (2020) 2258.
29. P. Song, H. Wang, L. Kang, B. Ran, H. Song and R. Wang, *Chem. Commun.*, 55 (2019) 687.
30. Y. Zhou, G. Zhang, M. Yu, X. Wang, J. Lv and F. Yang, *Acs Sustainable Chem. Eng.*, 6 (2018) 8437.
31. X. Li, X. Ren, X. Liu, J. Zhao, X. Sun, Y. Zhang, X. Kuang, T. Yan, Q. Wei and D. Wu, *J. Mater. Chem. A*, 7 (2019) 2524.
32. X. Li, X. Sun, L. Zhang, S. Sun and W. Wang, *J. Mater. Chem. A*, 6 (2018) 3005.
33. K. Chu, Y.-P. Liu, Y.-B. Li, H. Zhang and Y. Tian, *J. Mater. Chem. A*, 7 (2019) 4389.
34. C. J. M. van der Ham, M. T. M. Koper and D. G. H. Hetterscheid, *Chem. Soc. Rev.*, 43 (2014) 5183.
35. J. Zhao and Z. Chen, *J. Am. Chem. Soc.*, 139 (2017) 12480.
36. Y.-J. Tang, Y. Wang, X.-L. Wang, S.-L. Li, W. Huang, L.-Z. Dong, C.-H. Liu, Y.-F. Li and Y.-Q. Lan, *Adv. Energy Mater.*, 6 (2016) 1600116.
37. D. Zhu, L. Zhang, R. E. Ruther and R. J. Hamers, *Nat. Mater.*, 12 (2013) 836.
38. G. W. Watt and J. D. Chrisp, *Anal. Chem.*, 24 (1952) 2006.
39. A S. Batchellor and S. W. Boettcher, *ACS Catal.*, 5 (2015) 6680.
40. W. Qiu, X.-Y. Xie, J. Qiu, W.-H. Fang, R. Liang, X. Ren, X. Ji, G. Cui, A. M. Asiri, G. Cui, B. Tang and X. Sun, *Nat. Commun.*, 9 (2018) 3485.
41. X. Ren, J. Zhao, Q. Wei, Y. Ma, H. Guo, Q. Liu, Y. Wang, G. Cui, A. M. Asiri, B. Li, B. Tang and X. Sun, *ACS Cent. Sci.*, 5 (2019) 116.
42. P. Song, H. Wang, L. Kang, B. Ran, H. Song and R. Wang, *Chem. Commun.*, 55 (2019) 687.
43. H. Huang, L. Xia, X. Shi, A. M. Asiri and X. Sun, *Chem. Commun.*, 54 (2018) 11427.
44. V. Kordali, G. Kyriacou and C. Lambrou, *Chem. Commun.*, 17 (2000) 1673.
45. H. Huang, L. Xia, R. Cao, Z. Niu, H. Chen, Q. Liu, T. Li, X. Shi, A. M. Asiri and X. Sun, *Chem. Eur. J.*, 25 (2018) 1914.
46. J. Yu, C. Li, B. Li, X. Zhu, R. Zhang, L. Ji, D. Tang, A. M. Asiri, X. Sun, Q. Li, S. Liu and Y. Luo, *Chem. Commun.*, 55 (2019) 6401.

47. D. Wu, H. Wang, H. Huang, R. Zhang, L. Ji, H. Chen, Y. Luo, J. You, D. Tang, Z. Zhang and X. P. Sun, *Chem. Commun*., 55 (2019) 7546.
48. W. Kong, Z. Liu, J. Han, L. Xia, Y. Wang, Q. Liu, X. Shi, Y. Wu, Y. Xu and X. Sun, *Inorg. Chem. Front*., 6 (2019) 423.
49. Z. Wang, Y. Li, H. Yu, Y. Xu, H. Xue, X. Li, H. Wang and L. Wang, *ChemSusChem*, 11 (2018) 3480.
50. Q. Liu, X. Zhang, B. Zhang, Y. Luo, G. Cui, F. Xie and X. Sun, *Nanoscale,* 10 (2018) 14386.
51. H. Yu, Z. Wang, D. Yang, X. Qian, Y. Xu, X. Li, H. Wang and L. Wang*, J. Mater. Chem*. A, 7 (2019) 12526.
52. H. Du, X. Guo, R.-M. Kong and F. L. Qu, *Chem. Commun*., 54 (2018) 12848.
53. S. Zhang, C. Zhao, Y. Liu, W. Li, J. Wang, G. Wang, Y. Zhang, H. Zhang and H. Zhao, *Chem. Commun.*, 55 (2019) 2952.
54. K. Jia, Y. Wang, L. Qiu, J. Gao, Q. Pan, W. Kong, X. Zhang, A. A. Alshehri, K. A. Alzahrani, B. Zhong, X. Guo and L. Yang, *Inorg. Chem. Front*., 6 (2019) 1986.